Research Article | Vol. 29, No. 7 / 29 March 2021 / Optics Express 10726
Optics EXPRESS

Influence of polarization directions of the IR+XUV two-color laser fields on angle-resolved photoelectron energy spectrum

FACHENG JIN,[1,2,3,6] HUIHUI YANG,[2] HONGDAN ZHANG,[1,3] BINGBING WANG,[4,7] AND WEIFENG YANG[1,3,5,8]

[1]Research Center for Advanced Optics and Photoelectronics, Department of Physics, College of Science, Shantou University, Shantou, Guangdong 515063, China
[2]Faculty of Science, Xi'an Aeronautical University, Xi'an 710077, China
[3]Department of Mathematics, College of Science, Shantou University, Shantou, Guangdong 515063, China
[4]Laboratory of Optical Physics, Beijing National Laboratory for Condensed Matter Physics, Institute of Physics, Chinese Academy of Sciences, Beijing 100190, China
[5]Key Laboratory of Intelligent Manufacturing Technology, Ministry of Education, Shantou University, Shantou, Guangdong 515063, China
[6]fchjin@163.com
[7]wbb@aphy.iphy.ac.cn
[8]wfyang@stu.edu.cn

Abstract: By employing the frequency-domain theory, we investigate the influence of polarization directions on angle-resolved photoelectron energy spectrum in the above-threshold ionization (ATI) process of atoms exposed to the IR+XUV two-color laser fields, which shows the multiplateau structures. When the ionized electron is emitted along the IR laser's polarization direction, the width of each plateau keeps a certain energy range, and the jet structures and main lobes are determined by both the emission angle relative to the polarization direction of the XUV laser field and the number of the XUV photons absorbed by the electron. While when the ionized electron is emitted along the XUV laser's polarization direction, the width of each plateau depends on the polarization direction of the IR laser field, and the angular distribution of the ionized electron exhibits the isotropic characteristics. These results show that the ATI spectrum may be effectively controlled by changing the angle between the two laser fields' polarization directions.

1. Introduction

The interaction of matter and an intense laser field triggers various interesting phenomena, such as above-threshold ionization (ATI) [1–3], high-order harmonic generation (HHG) [4,5] and double ionization [6,7]. The ATI is one of the fundamental processes in the strong-field physics. So far, the ATI process has been extensively studied since its first experimental observation [8]. In this process, an electron can absorb much more photons than the minimum photon number necessary to overcome the ionization potential. The ATI spectrum encodes the information about the structure of atoms or molecules, as well as laser fields, which can uncover the underlying dynamics process [9–13]. Generally, the spectrum may consist of the low-energy and high-energy parts, which correspond to the direct ATI and high-order ATI (HATI) processes separately. The HATI process can be explained by the three-step model [14–16]. It was demonstrated that the low-energy spectrum obviously depends on the laser intensity [9,17,18], and it is also attributed to the Coulomb potential [19–21]. Recently, the carrier-envelope-phase (CEP) control of asymmetries in the ATI of xenon atoms exposed to ultrashort bichromatic fields was investigated [22]. Therefore, the ATI spectrum can be used to detect the CEP of the incident laser field [23], as well as the structures of atom and molecule [24–26].

#420316 https://doi.org/10.1364/OE.420316
Journal © 2021 Received 25 Jan 2021; revised 19 Feb 2021; accepted 8 Mar 2021; published 22 Mar 2021

Optics EXPRESS

With the development of the free-electron laser technology [27,28] and the application of HHG [29,30], the extreme ultraviolet (XUV) and the infrared (IR) two-color laser fields have become an efficient tool to investigate the strong-field physics community [31–36]. The different types of dichroism in shortpulse two-color XUV+IR multiphoton ionization were analyzed, especially for the circular dichroism [35,37–39]. The asymmetric structure of the ATI spectrum of an atom in two-color elliptically polarized laser fields was studied [40]. The first experimental investigation of linear dichroism in two-color XUV+IR ionization of He atom was performed [41], which shows that the formation of the sideband structures depends differently on the relative orientation of the IR and XUV polarization vectors. The investigations on the angular distribution of photoelectron and angle-resolved photoelectron energy spectrum are in favor of the analysis of the dichroism. The angle-resolved energy distribution of photoelectrons was studied when both lasers are linearly polarized along the same polarization direction [42]. When the energy of an XUV photon is much more than the atomic ionization potential, the angle-resolved energy distribution of photoelectrons presented a multiplateau structure [34–36,43,44]. The angular resolved ATI spectrum in IR+XUV orthogonally polarized two-color laser fields was discussed [45], which showed the dip structures of different plateaus. In recent experiments, it was shown that the amplitude of the sidebands varies strongly with the emission angle, and the angular distribution pattern is attributed to interferences between the different angular momenta for the emission electron in the multiphoton process [46]. It was further experimentally found that the photoelectron angular distribution strongly depends on the orientation of the IR polarization plane with respect to that of the XUV field [47]. These studies show that the angular distribution of the ionized electron depends on the polarization directions of two lasers and the emission directions of electron.

In this paper, by employing the frequency-domain theory based on the nonperturbative quantum electrodynamics [48,49], we will discuss the angle-resolved PES in the ATI process of atoms exposed to the IR+XUV two-color laser fields. Comparing with the time-dependent theory (e.g. TDSE), in this approach there are three advantages to deal with the strong-field physics [50]. Firstly, the key feature of this theory is time-independent, which can greatly save the computation time. Secondly, this approach provides a different concept for the physical processes of the strong-field, especially for recollision process (e.g. HATI, NSDI, HHG), which can generally be treated as a direct ATI followed by a laser-assisted collision or laser-assisted recombination so as to investigate the role of these subprocesses separately. Thirdly, all of the recollision processes can be investigated under a unified theoretical frame, which is in favor of analyzing the relationship among all these recollision processes. However, the investigation addressing the influence of the polarization directions on the ATI process is rare in detail. Here we will investigate the influence of polarization directions on angle-resolved PES in the ATI process of atoms exposed to the IR+XUV two-color laser fields. It is found that the formation of the spectrum depends on the angle between the emission direction of the ionized electron and polarization direction of the XUV laser field.

Atomic units are used throughout unless otherwise stated.

2. Theoretical method

In the frequency-domain theory based on the nonperturbative quantum electrodynamics, the transition matrix from the initial state $|\Psi_i\rangle$ to the final state $|\Psi_f\rangle$ in the ATI process can be expressed as [49]

$$T_{fi} = \langle \Psi_f | V | \Psi_i \rangle, \tag{1}$$

where V represents the potential of interaction between the electron and two laser fields, which can be expressed by $V = -[(-i\nabla)\cdot\mathbf{A}_1(-\mathbf{k}_1\cdot\mathbf{r}) + (-i\nabla)\cdot\mathbf{A}_2(-\mathbf{k}_2\cdot\mathbf{r}) + \mathbf{A}_1(-\mathbf{k}_1\cdot\mathbf{r})\cdot(-i\nabla) + \mathbf{A}_2(-\mathbf{k}_2\cdot\mathbf{r})\cdot(-i\nabla)]/2 + [\mathbf{A}_1(-\mathbf{k}_1\cdot\mathbf{r}) + \mathbf{A}_2(-\mathbf{k}_2\cdot\mathbf{r})]^2/2$. Here $\mathbf{A}_\gamma(-\mathbf{k}_\gamma\cdot\mathbf{r}) = (2\omega_\gamma V_\gamma)^{-1/2}[\hat{\epsilon}_\gamma \exp(i\mathbf{k}_\gamma\cdot\mathbf{r})a_\gamma + c.c.]$, $\mathbf{k}_\gamma$ is the wave vector, $a_\gamma(a_\gamma^+)$ is the annihilation (creation) operator, V_γ is the normalization

Optics EXPRESS

volume of the laser field, and $\hat{\epsilon}_\gamma = [\varepsilon_x \cos(\xi_\gamma/2) + i\varepsilon_y \sin(\xi_\gamma/2)] \exp[i\phi_\gamma/2]$ is the polarization vector, ϕ_γ is the initial phase of the two laser fields of the laser frequency ω_γ, the angle ξ_γ is the degree of polarization, $\xi_\gamma = 0$ corresponds to the linear polarization for $\gamma = 1$ or 2. The initial state $|\Psi_i\rangle$ can be written as

$$|\Psi_i\rangle = \Phi_i(\mathbf{r}) \otimes |n_1, n_2\rangle, \tag{2}$$

with the initial energy being $E_i = -I_p + (n_1 + 1/2)\omega_1 + (n_2 + 1/2)\omega_2$. Here $\Phi_i(\mathbf{r})$ is the ground state of the atom, $|n_1, n_2\rangle$ is the Fock state of the laser field with the photon number n_γ for γ =1 or 2, I_p is the ionization potential of the atom. Based on the strong-field approximation, the influence of the Coulomb potential of the ion on the ionized electron and the effect of the laser field on the bound electron in the ground state are neglected. The final state of system $|\Psi_f\rangle = |\Psi_{\mathbf{p}_f, q_1 q_2}(\mathbf{r})\rangle$ is the quantized-field Volkov state in the two-color laser fields, which can be expressed as [49]

$$\begin{aligned} |\Psi_{\mathbf{p}_f, q_1 q_2}(\mathbf{r})\rangle = V_e^{-1/2} \sum_{\substack{j_1=-q_1 \\ j_2=-q_2}}^{\infty} & \exp\{i[\mathbf{p}_f + (u_{p_1} - j_1)\mathbf{k}_1 + (u_{p_2} - j_2)\mathbf{k}_2] \cdot \mathbf{r}\} \\ & \times \aleph_{j_1 j_2}(\zeta_f)^* \exp[-i(j_1\phi_1 + j_2\phi_2)]|q_1 + j_1, q_2 + j_2\rangle, \end{aligned} \tag{3}$$

with the corresponding energy $E_f = {\mathbf{p}_f}^2/2 + (q_1 + 1/2)\omega_1 + (q_2 + 1/2)\omega_2 + u_{p_1}\omega_1 + u_{p_2}\omega_2$, where q_γ represents the background photons in the laser-matter system, j_γ represents the transferred photons with γ=1 or 2. Here $u_{p_\gamma} = \Lambda_\gamma^2/\omega_\gamma$ is the ponderomotive energy in units of the photon energy of the laser, where Λ_γ is the half amplitude of the classical field under the large photon number limit (i.e., $n_\gamma \to \infty$, $(2\omega_\gamma V_\gamma)^{-1/2} \to \infty$), and the intensity of the laser field $I_\gamma \to 2\Lambda_\gamma^2\omega_\gamma^2$ with γ=1 or 2. In Eq. (3), the generalized Bessel function can be written as

$$\begin{aligned} \aleph_{j_1 j_2}(\zeta_f) = \sum_{q_3 q_4 q_5 q_6} & J_{-j_1+2q_3+q_5+q_6}(\zeta_1) J_{-j_2+2q_4+q_5-q_6}(\zeta_2) \\ & \times J_{-q_3}(\zeta_3) J_{-q_4}(\zeta_4) J_{-q_5}(\zeta_5) J_{-q_6}(\zeta_6), \end{aligned} \tag{4}$$

where

$$\begin{aligned} \zeta_1 &= 2\sqrt{\frac{u_{p_1}}{\omega_1}}\mathbf{p}_f \cdot \widehat{\epsilon}_1, \qquad \zeta_2 = 2\sqrt{\frac{u_{p_2}}{\omega_2}}\mathbf{p}_f \cdot \widehat{\epsilon}_2, \\ \zeta_3 &= \frac{1}{2}u_{p_1}\widehat{\epsilon}_1 \cdot \widehat{\epsilon}_1, \qquad \zeta_4 = \frac{1}{2}u_{p_2}\widehat{\epsilon}_2 \cdot \widehat{\epsilon}_2, \\ \zeta_5 &= 2\frac{\sqrt{u_{p_1}\omega_1 u_{p_2}\omega_2}}{\omega_1 + \omega_2}\widehat{\epsilon}_1 \cdot \widehat{\epsilon}_2, \qquad \zeta_6 = 2\frac{\sqrt{u_{p_1}\omega_1 u_{p_2}\omega_2}}{\omega_1 - \omega_2}\widehat{\epsilon}_1 \cdot \widehat{\epsilon}_2. \end{aligned} \tag{5}$$

In the above, q_3, q_4, q_5 and q_6 can be considered dummy variables and be summed from $-\infty$ and ∞ [49]. By using Eqs. (2) and (3), the transition matrix for the ATI can be expressed as [43]

$$T_{fi} = V_e^{-1/2}(U_{p_1} + U_{p_2} - s_1\omega_1 - s_2\omega_2)\aleph_{s_1 s_2}(\zeta_f) \exp[i(s_1\phi_1 + s_2\phi_2)]\Phi(\mathbf{p}_f), \tag{6}$$

where $s_1 = n_1 - q_1$ and $s_2 = n_2 - q_2$ represent the photon numbers absorbed by electron from the two laser fields. In this paper, the initial state $\Phi(\mathbf{p}_f)$ of atom is approximated by the function of hydrogenlike atom in the momentum space.

3. Numerical results

In this section, we will consider the ATI process of an atom exposed to the IR+XUV two-color linearly polarized laser fields, where the atomic ionization potential is I_p = 12.1 eV. The frequencies of the IR and XUV laser fields are ω_1 = 1.165 eV and $\omega_2 = 20\omega_1$, and their initial phases are set to be zero for simplicity. Under the present lasers' conditions, we only consider the direct ATI process, because its contribution is much larger than the rescattering contributions.

Optics EXPRESS

Figure 1 shows the angle-resolved PESs for different laser intensities, where the ionized electron is emitted along the IR laser's polarization direction, and θ is the angle between the polarization directions of IR and XUV lasers. It can be seen that each of the PESs shows a multiplateau structure, where the probability of the first plateau is much larger than that of other plateaus, and there exist several minimum values (dip structures) in each plateau when the angle between the direction of emitted electron and the polarization of the XUV laser field changes. If the angle $\theta = 0^o$ or 180^o, the ATI spectrum will also show the terracelike structure similar with the previous results results [43]. Furthermore, for the electron emitted along the polarization of the IR laser field, it is found that the width of each plateau keeps a certain energy range. From Figs. 1(a)-(c) or (d)-(f), one can find that the width of each plateau increases with the intensity of the IR laser field, and even the overlap between the adjacent plateaus occurs. By comparing Figs. 1(a) and (d), it is shown that the ionization probability of the ATI process increases with the intensity of the XUV laser field, and the number of the plateaus also increases. It indicates that the IR and XUV laser fields play different roles in the ATI process, where the XUV laser field plays a crucial role to the ionization probability of the ATI process, and the IR laser field makes a dominant contribution to the width of each plateau, which are consistent with the cases in the IR+XUV orthogonally polarized two-color laser fields [45] and the experimental results [36].

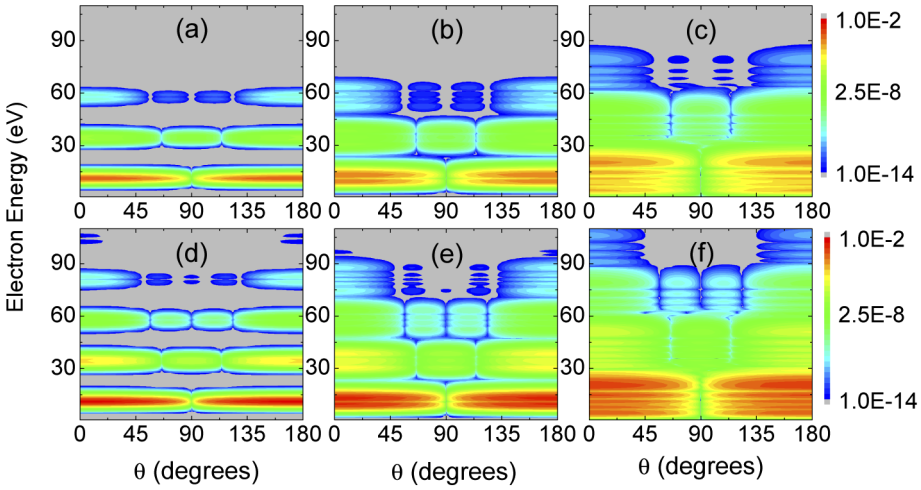

Fig. 1. The angle-resolved PESs as a function of the angle θ between polarization directions of the XUV and IR two-color laser fields, where the electron is emitted along the IR laser polarization direction. The XUV intensity of (a)-(c) is $I_2 = 3.6 \times 10^{13}$ W/cm^2, and its IR intensities are (a) $I_1 = 1.0 \times 10^{11}$ W/cm^2, (b) $I_1 = 1.0 \times 10^{12}$ W/cm^2 and (c) $I_1 = 1.0 \times 10^{13}$ W/cm^2; the XUV intensity of (d)-(f) is $I_2 = 3.6 \times 10^{14}$ W/cm^2, and its IR intensities are (d) $I_1 = 1.0 \times 10^{11}$ W/cm^2, (e) $I_1 = 1.0 \times 10^{12}$ W/cm^2, and (f) $I_1 = 1.0 \times 10^{13}$ W/cm^2. (on logarithmic scale).

Next we show the angle-resolved PESs for the ionized electron being emitted along the polarization of the XUV laser field, as shown in Fig. 2. It can be seen that each of these spectra also shows a muliplateau structure, the ionization probability of the ATI process increases with the intensity of the XUV laser field, while the width of each plateau increases with the intensity of the IR laser field. These results are consistent with the above results in Fig. 1. Furthermore, it is noticed that the width of the ionized electron energy strongly depends on the angle between the emission direction of the ionized electron and the polarization direction of the IR laser field. The width of each plateau decreases with the change from $\theta = 0^o$ (180^o) to 90^o, which is in well agreement with the experimental results [46]. Especially, the energy range is the largest for $\theta =$

Optics EXPRESS

0^o or 180^o, the energy range is the narrowest for $\theta = 90^o$. This result can be also observed in the experiment for the first plateau [47]. By comparison with Fig. 2 and Fig. 1, the width of each plateau is determined by the angle between the emission direction of the ionized electron and the polarization direction of the IR laser; while the minimum value is determined by the angle between the emission direction of the ionized electron and the polarization direction of the XUV laser.

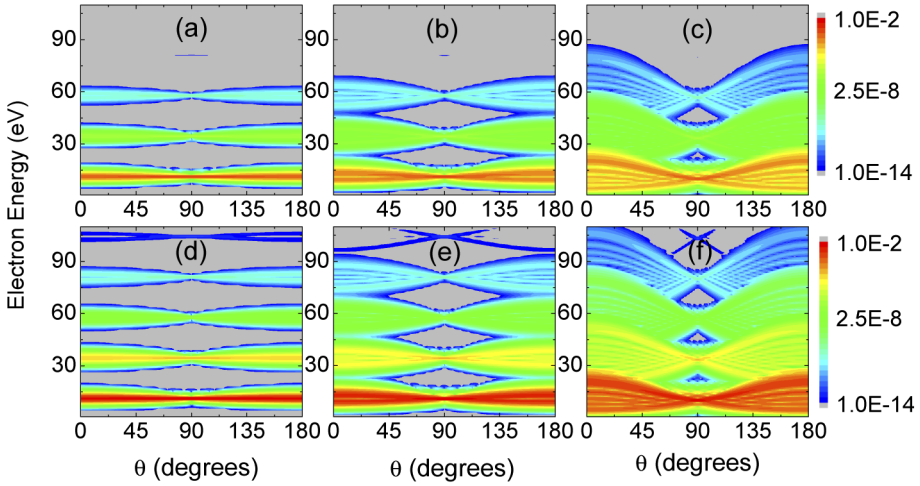

Fig. 2. The angle-resolved PESs as a function of the angle between polarization directions of the XUV and IR two-color laser fields, where the electron is emitted along the XUV laser polarization direction. The parameters of two laser fields are same as the case in Fig. 1. (on logarithmic scale).

In order to explain the reason of the formation of multiplateau structures shown in Figs. 1 and 2, we define the channel by the number s_2 of the XUV photons absorbed by the electron in the ATI process. Taking Fig. 1(b) as an example, Fig. 3 shows the channel contributions of atom absorbing one (a), two (b), and three (c) XUV photons, where other channels are not shown because of their little contributions. Comparing Fig. 3 and Fig. 1(b), the first, second and third plateaus in Fig. 1(b) are separately corresponding to the processes of atom absorbing one, two and three XUV photons. It indicates that the ionization probability rapidly decreases with an increase number of atom absorbing XUV photons. To explain the formation of Fig. 2(b), as an example, the corresponding channel contributions are shown in Fig. 4. One can see that the angle-resolved PES of Fig. 2(b) is also from contributions of atoms absorbing one, two and three XUV photons.

So as to understand the formation of each plateau in the angle-resolved PES, we will analyze the generalized Bessel function $\aleph_{s_1 s_2}(\zeta_f)$ in the transition matrix Eq. (6). In present laser conditions, the arguments of the generalized Bessel function $\zeta_i \approx 0.0$ for $i = 5$ and 6, hence we set $J_{s_i}(\zeta_i) \approx 1.0$ and $s_i = 0.0$ for $i = 5$ and 6. Therefore, the generalized Bessel function $\aleph_{s_1 s_2}(\zeta_f)$ can be reduced to [43]

$$\aleph_{s_1 s_2}(\zeta_f) \approx J_{-s_1}(\zeta_1, \zeta_3) J_{-s_2}(\zeta_2, \zeta_4), \tag{7}$$

where $J_{-s_1}(\zeta_1, \zeta_3) = \sum_{j_3} J_{-s_1+2j_3}(\zeta_1) J_{-j_3}(\zeta_3)$ and $J_{-s_2}(\zeta_2, \zeta_4) = \sum_{j_4} J_{-s_2+2j_4}(\zeta_2) J_{-j_4}(\zeta_4)$. One can find that $J_{-s_1}(\zeta_1, \zeta_3)$ is related to the IR laser field, and $J_{-s_2}(\zeta_2, \zeta_4)$ is related to the XUV laser field.

In the following, we will discuss the characters of each plateau caused by the IR laser field, which is determined by the Bessel function $J_{-s_1}(\zeta_1, \zeta_3)$. The ionized electron can absorb or emit many photons in the ATI process for an intense IR laser field. Hence the IR laser field can be

Optics EXPRESS

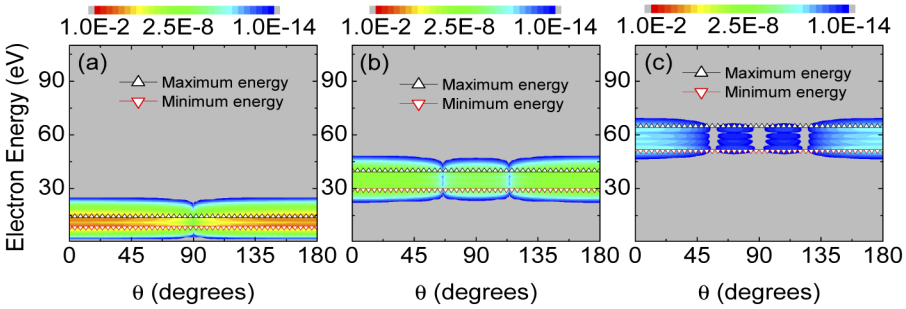

Fig. 3. Channel contributions of electron absorbing one (a), two (b) and three (c) XUV photons for the ionized electron being ionized along the polarization of the IR laser field $\varphi = 0$. The upper triangular and lower triangular curves are plotted by the expressions $E_{max} = [\sqrt{2(s_2\omega_2 - I_p) - 4U_{p_1} sin\varphi^2} + 2\sqrt{4U_{p_1}} cos\varphi]^2/2$ and $E_{min} = [\sqrt{2(s_2\omega_2 - I_p) - 4U_{p_1} sin\varphi^2} - 2\sqrt{4U_{p_1}} cos\varphi]^2/2$, respectively, indicating the maximal and minimal energies obtained by electron in the corresponding channel. The intensities of IR and XUV laser fields are $I_1 = 1.0 \times 10^{12}$W/cm^2 and $I_2 = 3.6 \times 10^{13}$W/cm^2. (on logarithmic scale).

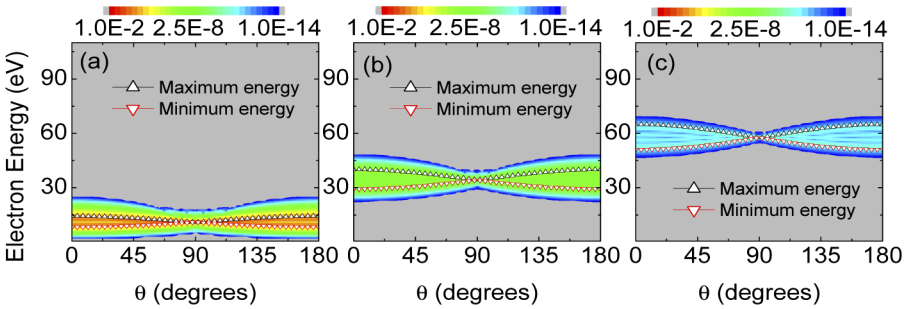

Fig. 4. Channel contributions of electron absorbing one (a), two (b) and three (c) XUV photons for the ionized electron being ionized along the polarization of the XUV laser field. The upper triangular and lower triangular curves indicate the maximal and minimal energies obtained by electron in the corresponding channel. The intensities of IR and XUV laser fields are $I_1 = 1.0 \times 10^{12}$ W/cm^2 and $I_2 = 3.6 \times 10^{13}$ W/cm^2. (on logarithmic scale).

treated as a classical field, $\mathbf{A}_{cl}(t) = \hat{\varepsilon}_1 E_1/\omega_1 \cos(\omega_1 t)$ with E_1 being the amplitude of the laser field. With the help of the saddle-point approximation, the ionization time t_0 satisfies the energy conservation relationship in the ATI process [45]

$$\frac{1}{2}[\mathbf{p}_f + \mathbf{A}_{cl}(t_0)]^2 = s_2\omega_2 - I_p, \tag{8}$$

where s_2 represents the number of XUV photons absorbed by the electron. Based on Eq. (8), if the angle φ between the emission direction of the ionized electron and polarization direction of the IR laser field is lower than 90^o, the maximum energy of ionized electron can be expressed as $E_{max} = [\sqrt{2(s_2\omega_2 - I_p) - 4U_{p_1} sin^2\varphi} + 2\sqrt{U_{p_1}} cos\varphi]^2/2$, and the minimum energy can be expressed as $E_{min} = [\sqrt{2(s_2\omega_2 - I_p) - 4U_{p_1} sin^2\varphi} - 2\sqrt{U_{p_1}} cos\varphi]^2/2$. If φ is larger than 90^o, the maximum and minimum positions exchange. When the ionized electron is emitted along the IR laser field, here the corresponding maximum and minimum positions are shown by the upper and lower triangular curves in Figs. 3(a)-(c). Also, as the ionized electron is emitted along the XUV laser field, the corresponding maximum and minimum positions are shown by the

Optics EXPRESS

upper and lower triangular curves in Figs. 4(a)-(c). One can see that the classical results agree well with the quantum calculations. These results indicate that the ATI process of atoms in the IR+XUV two-color laser fields can be considered as following: the multiphoton ionization occurs by electron absorbing s_2 photons from the XUV laser field, which leads to the emergence of multiplateau structures; and then the ionized electron can be accelerated or decelerated by the IR laser field, leading to the formation for width of each plateau, where the energy range is equal to $\Delta E = 4\sqrt{[2(s_2\omega_2 - I_p) - 4U_{p_1}sin^2\varphi]U_{p_1}cos\varphi}$, which depends on the angle φ between the emssion direction of the ionized electron and polarization direction of the IR laser field. It indicates that the energy width of each plateau is determined by the projection of the interaction between electron and the IR laser field on the polarization direction of the IR laser field. Especially, as the electron is emitted along the IR laser field i.e. $\varphi = 0$, the range of energy remains unchanged $\Delta E = 4\sqrt{2(s_2\omega_2 - I_p)U_{p_1}}$. In Fig. 3, the ranges of energy ΔE for the first, second and third plateaus are 6.16 eV, 10.80 eV, and 13.98 eV, respectively.

Figure 5 shows the ATI spectra as a function of the angle between the polarization directions of the two laser fields when the electron is emitted along the direction of the IR [(a)-(c)] or XUV [(d)-(f)] laser field. In Fig. 5(a), one can see that the ionized electron emitted along the polarization direction of the XUV laser field forms the main lobes, which is similar to the experimental result of the monochromatic XUV laser field [47]. It is noticed that the ionization probability of the ionized electron along the IR polarization is very low when the XUV polarization is perpendicular. This phenomenon had been explained by a zero point of the generalized Bessel function $\aleph_{s_1 s_2}(\zeta_f)$ [45] and the selection rule [51]. In Figs. 5(b) and (c), the jet structures appear between the main lobes. For electron absorbing even XUV photons, there exists a central jet; while for electron absorbing odd XUV photons, there is no central jet, and there are side jets in the case of electron absorbing three XUV photons. This result agrees with the experimental results in the monochromatic IR laser field [52,53]. On the other hand, when the ionized electron is emitted along the XUV laser field as shown in Figs. 5(d)-(f), the ATI spectra are independent of the the angle and exhibits the isotropic characteristics, no matter the number of XUV photons absorbed by the ionized electron is odd or even. As can be seen from Fig. 5, the jet structures in the ATI spectra are determined by both the angle between emission direction of the ionized electron and polarization direction of the XUV laser field and the number of photons absorbed by the emitted electron.

The features of the ATI spectra in Fig. 5 are caused by the XUV laser field, we analyze the Bessel function $J_{-s_2}(\zeta_2, \zeta_4)$ in Eq. (7). The parity property of the Bessel function is related to its order s_2 because of $J_{-s_2}(\zeta_2, \zeta_4) = (-1)^{s_2} J_{s_2}(\zeta_2, \zeta_4)$. It indicates that the angular distribution for electron absorbing even XUV photons has a central jet, while the angular distribution for electron absorbing odd photons has no central jet.

Figure 6 presents the Bessel function $|J_{-s_2}(|\zeta|, \zeta_4)|^2$ as a function of the variable $|\zeta|$ for s_2 =1(a), 2(b) and 3(c), respectively. In Fig. 6(a), when $|\zeta| = 0.0$, $J_{-s_2}(|\zeta|, \zeta_4) \approx 0.0$, which leads to the disappearance of the central jet; then the Bessel function increases with $|\zeta|$, which leads to the formation of the main lobes. In Fig. 6(b), there exists a maximum value at $|\zeta| = 0.0$, while there is a minimum value at $|\zeta| \approx 0.03$. The change from $|\zeta| = 0.0$ to 0.03 leads to the formation of the central jet, and the formation of the main lobes comes from $|\zeta|$>0.03. In Fig. 6(c), the interval $[0, 0.048]$ of $|\zeta|$ leads to the side jets, and the interval $[0.048, 0.09]$ leads to the main lobes. As the order s_2 increases, the number of the minimum values of the Bessel function also increases, and these minimum values are sources of the dip structures in Fig. 1. Hence the jet structures and main lobes are determined by both the emission angle relative to the polarization direction of the XUV laser field and the number of the XUV photons that the electron absorbs.

Optics EXPRESS

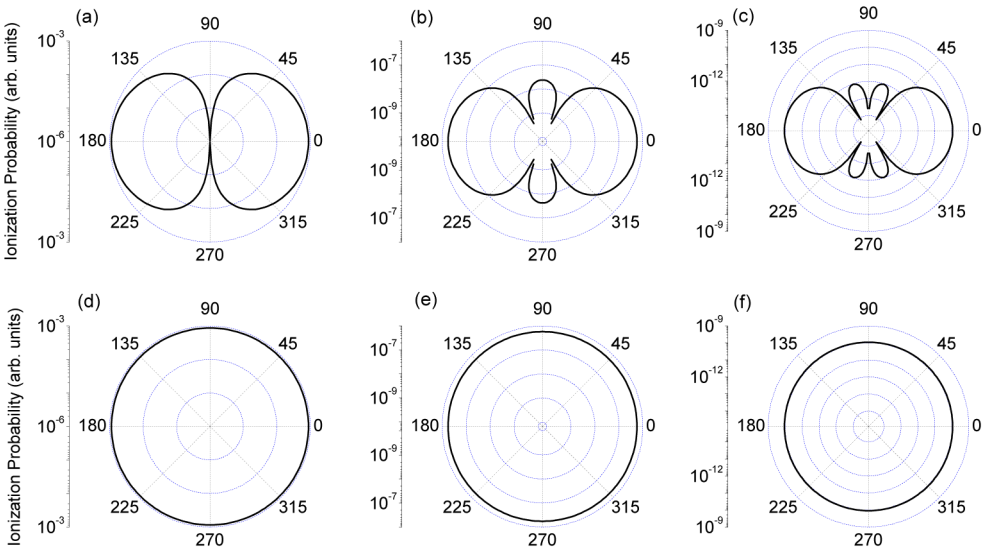

Fig. 5. The ATI spectra of the ionized electron as a function of the angle between the polarization directions of two lasers for the first [(a), (d)], second [(b), (e)] and third [(c), (f)] plateaus, when the ionized electron is emitted along the polarizations of the IR [(a)-(c)] and XUV [(d)-(f)] laser fields. The laser intensities for [(a)-(c)] and [(d)-(f)] are same as the parameters in Figs. 3 and 4, respectively.

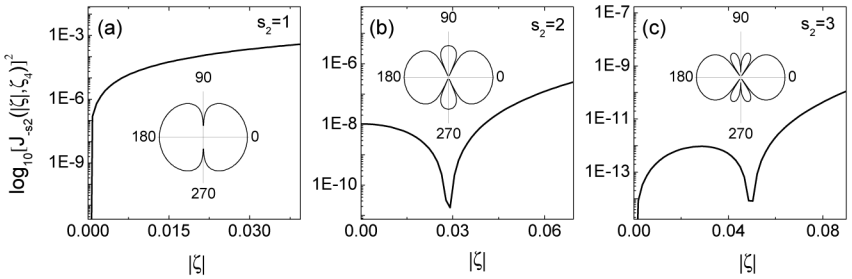

Fig. 6. The Bessel function $|J_{-s_2}(|\zeta|, \zeta_4)|^2$ as a function of the variable $|\zeta|$ for s_2 =1(a), 2(b) and 3(c), respectively. The insets are the calculated angular distributions of $|J_{-s_2}(|\zeta|, \zeta_4)|^2$. $|\zeta| = 2\sqrt{2u_{p_2}(s_2\omega_2 - U_{p_1} - U_{p_2} - I_p)/\omega_2}|\cos\theta|$. The laser intensities are same as the parameters in Fig. 3.

4. Conclusion

In this paper, we have investigated the influence of polarization directions of two laser fields on the angle-resolved PES in the ATI process of atoms exposed to the IR+XUV two-color laser fields. The IR and XUV laser fields play different roles in the ATI process, where the IR laser field determines the width of each plateau, and the XUV laser field plays a crucial role for ionization probability. The angle-resolved PES shows the multiplateau structure. When the ionized electron is emitted along the IR laser's polarization direction, the energy width of each plateau remains unchanged, and the jet structures in the ATI spectrum are determined by both the angle between direction of the emitted electron and polarization direction of the XUV laser field and the number of the photons that the electron absorbs. When the ionized electron is emitted along the XUV laser's polarization direction, the width of each plateau is mainly determined by the angle between the emission direction of the ionized electron and the polarization direction of

Optics EXPRESS

the IR laser, and the ATI spectrum shows the isotropic characteristics. Furthermore, by analyzing of the generalized Bessel function, it is found that the energy width of each plateau can be treated as the projection of the interaction between electron and the IR laser field on the polarization direction of the IR laser field. The angular distribution for electron absorbing even XUV photons has a central jet, while the angular distribution for electron absorbing odd photons has no central jet.

Funding. National Natural Science Foundation of China (11947080, 11804264, 11774215, 11774411, 12074418, 91950101).

Disclosures. The authors declare no conflicts of interest.

References

1. W. Becker, F. Grasbon, R. Kopold, D. B. Milošević, G. G. Paulus, and H. Walther, "Above-Threshold Ionization: From Classical Features to Quantum Effects," Adv. At., Mol., Opt. Phys. **48**, 35–98 (2002).
2. X. Gong, C. Lin, F. He, Q. Song, K. Lin, Q. Ji, W. Zhang, J. Ma, P. Lu, Y. Liu, H. Zeng, W. Yang, and J. Wu, "Energy-Resolved Ultrashort Delays of Photoelectron Emission Clocked by Orthogonal Two-Color Laser Fields," Phys. Rev. Lett. **118**(14), 143203 (2017).
3. M.-H. Yuan and X.-B. Bian, "Angular distribution of photoelectron momentum in above-threshold ionization by circularly polarized laser pulses," Phys. Rev. A **101**(1), 013412 (2020).
4. L. Liu, J. Zhao, W. Dong, J. Liu, Y. Huang, and Z. Zhao, "Spatial coherence in high-order-harmonic generation from periodic solid structures," Phys. Rev. A **96**(5), 053403 (2017).
5. Y. Qiao, D. Wu, J.-G. Chen, J. Wang, F.-M. Guo, and Y.-J. Yang, "High-order harmonic generation from H_2^+ irradiated by a co-rotating two-color circularly polarized laser field," Phys. Rev. A **100**(6), 063428 (2019).
6. S.-G. Chen, W.-C. Jiang, S. Grundmann, F. Trinter, M. S. Schöffler, T. Jahnke, R. Dörner, H. Liang, M.-X. Wang, L.-Y. Peng, and Q. Gong, "Photon Momentum Transfer in Single-Photon Double Ionization of Helium," Phys. Rev. Lett. **124**(4), 043201 (2020).
7. F. Sun, X. Chen, W. Zhang, J. Qiang, H. Li, P. Lu, X. Gong, Q. Ji, K. Lin, H. Li, J. Tong, F. Chen, C. Ruiz, J. Wu, and F. He, "Longitudinal photon-momentum transfer in strong-field double ionization of argon atoms," Phys. Rev. A **101**(2), 021402 (2020).
8. P. Agostini, F. Fabre, G. Mainfray, G. Petite, and N. K. Rahman, "Free-Free Transitions Following Six-Photon Ionization of Xenon Atoms," Phys. Rev. Lett. **42**(17), 1127–1130 (1979).
9. M. Li, Y. Liu, H. Liu, Y. Yang, J. Yuan, X. Liu, Y. Deng, C. Wu, and Q. Gong, "Photoelectron angular distributions of low-order above-threshold ionization of Xe in the multiphoton regime," Phys. Rev. A **85**(1), 013414 (2012).
10. R. Della Picca, A. A. Gramajo, C. R. Garibotti, S. D. Lopez, and D. G. Arbo, "Nonconstant ponderomotive energy in above-threshold ionization by intense short laser pulses," Phys. Rev. A **93**(2), 023419 (2016).
11. X. Song, G. Shi, G. Zhang, J. Xu, C. Lin, J. Chen, and W. Yang, "Attosecond Time Delay of Retrapped Resonant Ionization," Phys. Rev. Lett. **121**(10), 103201 (2018).
12. X. Liu, G. Zhang, J. Li, G. Shi, M. Zhou, B. Huang, Y. Tang, X. Song, and W. Yang, "Deep Learning for Feynman's Path Integral in Strong-Field Time-Dependent Dynamics," Phys. Rev. Lett. **124**(11), 113202 (2020).
13. K.-J. Yuan and A. D. Bandrauk, "Above-threshold ionization in molecules by intense multiple-frequency circularly polarized laser pulses," Phys. Rev. A **98**(2), 023413 (2018).
14. F. Krausz and M. Ivanov, "Attosecond physics," Rev. Mod. Phys. **81**(1), 163–234 (2009).
15. P. B. Corkum, "Plasma perspective on strong field multiphoton ionization," Phys. Rev. Lett. **71**(13), 1994–1997 (1993).
16. L. Guo, S. Chen, M. Liu, Z. Shu, S. Hu, R. Lu, S. Han, and J. Chen, "Rescattering time-energy analysis of high-order above-threshold ionization in few-cycle laser fields," Phys. Rev. A **101**(3), 033415 (2020).
17. C. M. Maharjan, A. S. Alnaser, I. Litvinyuk, P. Ranitovic, and C. L. Cocke, "Wavelength dependence of momentum-space images of low-energy electrons generated by short intense laser pulses at high intensities," J. Phys. B: At., Mol. Opt. Phys. **39**(8), 1955–1964 (2006).
18. D. G. Arbó, K. I. Dimitriou, E. Persson, and J. Burgdörfer, "Sub-Poissonian angular momentum distribution near threshold in atomic ionization by short laser pulses," Phys. Rev. A **78**(1), 013406 (2008).
19. S. Xu, W. Quan, Y. Chen, Z. Xiao, Y. Wang, H. Kang, L. Hua, C. Gong, X. Lai, X. Liu, X. Hao, S. Hu, and J. Chen, "Long-range Coulomb effect in above-threshold ionization of Ne subject to few-cycle and multicycle laser fields," Phys. Rev. A **95**(6), 063405 (2017).
20. A. Rudenko, K. Zrost, C. D. Schröter, V. L. B de Jesus, B. Feuerstein, R. Moshammer, and J. Ullrich, "Resonant structures in the low-energy electron continuum for single ionization of atoms in the tunnelling regime," J. Phys. B: At., Mol. Opt. Phys. **37**(24), L407–L413 (2004).
21. D. G. Arbó, S. Yoshida, E. Persson, K. I. Dimitriou, and J. Burgdröfer, "Interference Oscillations in the Angular Distribution of Laser-Ionized Electrons near Ionization Threshold," Phys. Rev. Lett. **96**(14), 143003 (2006).
22. S. Kerbstadt, D. Pengel, L. Englert, T. Bayer, and M. Wollenhaupt, "Carrier-envelope-phase control of asymmetries in the multiphoton ionization of xenon atoms by ultrashort bichromatic fields," Phys. Rev. A **97**(6), 063402 (2018).

Optics EXPRESS

23. X. M. Tong, K. Hino, and N. Toshima, "Phase-dependent atomic ionization in few-cycle intense laser fields," Phys. Rev. A **74**(3), 031405 (2006).
24. Y. Guo, P. Fu, Z.-C. Yan, J. Gong, and B. Wang, "Imaging the geometrical structure of the H_2^+ molecular ion by high-order above-threshold ionization in an intense laser field," Phys. Rev. A **80**(6), 063408 (2009).
25. K.-J. Yuan and A. D. Bandrauk, "Angle-dependent molecular above-threshold ionization with ultrashort intense linearly and circularly polarized laser pulses," Phys. Rev. A **84**(1), 013426 (2011).
26. E. V. van der Zwan and M. Lein, "Molecular Imaging Using High-Order Harmonic Generation and Above-Threshold Ionization," Phys. Rev. Lett. **108**(4), 043004 (2012).
27. D. Gauthier, E. Allaria, M. Coreno, I. Cudin, H. Dacasa, M. B. Danailov, A. Demidovich, S. D. Mitri, B. Diviacco, E. Ferrari, P. Finetti, F. Frassetto, D. Garzella, S. Kunzel, V. Leroux, B. Mahieu, N. Mahne, M. Meyer, T. Mazza, P. Miotti, G. Penco, L. Raimondi, P. R. Ribic, R. Richter, E. Roussel, S. Schulz, L. Sturari, C. Svetina, M. Trovo, P. A. Walker, M. Zangrando, C. Callegari, M. Fajardo, L. Poletto, P. Zeitoun, L. Giannessi, and G. D. Ninno, "Chirped pulse amplification in an extreme-ultraviolet free-electron laser," Nat. Commun. **7**(1), 13688 (2016).
28. E. Allaria, R. Appio, L. Badano, A. W. Barletta, S. Bassanese, G. S. Biedron, A. Borga, E. Busetto, D. Castronovo, P. Cinquegrana, S. Cleva, D. Cocco, M. Cornacchia, P. Craievich, I. Cudin, G. D'Auria, M. Dal Forno, B. M. Danailov, R. De Monte, G. De Ninno, P. Delgiusto, A. Demidovich, S. Di Mitri, B. Diviacco, A. Fabris, R. Fabris, W. Fawley, M. Ferianis, E. Ferrari, S. Ferry, L. Froehlich, P. Furlan, G. Gaio, F. Gelmetti, L. Giannessi, M. Giannini, R. Gobessi, R. Ivanov, E. Karantzoulis, M. Lonza, A. Lutman, B. Mahieu, M. Milloch, V. S. Milton, M. Musardo, I. Nikolov, S. Noe, F. Parmigiani, G. Penco, M. Petronio, L. Pivetta, M. Predonzani, F. Rossi, L. Rumiz, A. Salom, C. Scafuri, C. Serpico, P. Sigalotti, S. Spampinati, C. Spezzani, M. Svandrlik, C. Svetina, S. Tazzari, M. Trovo, R. Umer, A. Vascotto, M. Veronese, R. Visintini, M. Zaccaria, D. Zangrando, and M. Zangrando, "Highly coherent and stable pulses from the FERMI seeded free-electron laser in the extreme ultraviolet," Nat. Photonics **6**(10), 699–704 (2012).
29. J. Heslar and S. I. Chu, "Probing multirescattering dynamics and electron quantum paths for below- and near-threshold harmonic generation of H_2 in an intense laser field," Phys. Rev. A **95**(4), 043414 (2017).
30. S. A. Berman, J. Dubois, C. Chandre, M. Perin, and T. Uzer, "Coherent buildup of high-order harmonic radiation: The classical perspective," Phys. Rev. A **97**(6), 061402 (2018).
31. S. X. Hu, "Boosting Photoabsorption by Attosecond Control of Electron Correlation," Phys. Rev. Lett. **111**(12), 123003 (2013).
32. F. Jin, Y. Tian, J. Chen, Y. Yang, X. Liu, Z.-C. Yan, and B. Wang, "Nonsequential double ionization of helium in IR+XUV two-color laser fields:Collision-ionization process," Phys. Rev. A **93**(4), 043417 (2016).
33. F. Jin, J. Chen, Y. Yang, Z.-C. Yan, and B. Wang, "Intensity dependence of nonsequential double ionization of helium in IR+XUV two-color laser fields," J. Phys. B: At., Mol. Opt. Phys. **49**(19), 195602 (2016).
34. A. K. Kazansky, I. P. Sazhina, and N. M. Kabachnik, "Influence of the partial temporal coherence of short FEL pulses on two-colour photoionization and photoinduced Auger decay of atoms," J. Phys. B: At., Mol. Opt. Phys. **46**(2), 025601 (2013).
35. A. K. Kazansky, I. P. Sazhina, and N. M. Kabachnik, "Angle-resolved electron spectra in short-pulse two-color XUV+ IR photoionization of atoms," Phys. Rev. A **82**(3), 033420 (2010).
36. P. Radcliffe, M. Arbeiter, W. B. Li, S. Düsterer, H. Redlin, P. Hayden, P. Hough, V. Richardson, J. T. Costello, T. Fennel, and M. Meye, "Atomic photoionization in combined intense XUV free-electron and infrared laser fields," New J. Phys. **14**(4), 043008 (2012).
37. A. K. Kazansky, A. V. Grigorieva, and N. M. Kabachnik, "Dichroism in short-pulse two-color XUV plus IR multiphoton ionization of atoms," Phys. Rev. A **85**(5), 053409 (2012).
38. R. Taïeb, V. Véniard, A. Maquet, N. L. Manakov, and S. I. Marmo, "Circular dichroism from unpolarized atoms in multiphoton multicolor ionization," Phys. Rev. A **62**(1), 013402 (2000).
39. T. Mazza, M. Ilchen, A. J. Rafipoor, C. Callegari, P. Finetti, O. Plekan, K. C. Prince, R. Richter, A. Demidovich, C. Grazioli, L. Avaldi, P. Bolognesi, M. Coreno, P. O'Keeffe, M. Di Fraia, M. Devetta, Y. Ovcharenko, V. Lyamayev, S. Dusterer, K. Ueda, J. T. Costello, E. V. Gryzlova, S. I. Strakhova, A. N. Grum-Grzhimailo, A. V. Bozhevolnov, A. K. Kazansky, N. M. Kabachnik, and M. Meyer, "Angular distribution and circular dichroism in the two-colour XUV+NIR above-threshold ionization of helium," J. Mod. Opt. **63**(4), 367–382 (2016).
40. X.-C. Zhou, S. Shi, F. Li, Y.-J. Yang, J. Chen, Q.-T. Meng, and B.-B. Wang, "Asymmetric structure of atomic above-threshold ionization spectrum in two-color elliptically polarized laser fields," Chin. Phys. B **28**(10), 103201 (2019).
41. M. Meyer, D. Cubaynes, D. Glijer, J. Dardis, P. Hayden, P. Hough, V. Richardson, E. T. Kennedy, J. T. Costello, P. Radcliffe, S. Düsterer, A. Azima, W. B. Li, H. Redlin, J. Feldhaus, R. Taïeb, A. Maquet, A. N. Grum-Grzhimailo, E. V. Gryzlova, and S. I. Strakhova, "Polarization Control in Two-Color Above-Threshold Ionization of Atomic Helium," Phys. Rev. Lett. **101**(19), 193002 (2008).
42. A. A. Gramajo, R. Della Picca, S. D. López, and D. G. Arbó, "Intra- and intercycle interference of angleresolved electron emission in laser-assisted XUV atomic ionization," J. Phys. B: At., Mol. Opt. Phys. **51**(5), 055603 (2018).
43. K. Zhang, J. Chen, X.-L. Hao, P. Fu, Z.-C. Yan, and B. Wang, "Terracelike structure in the above-threshold-ionization spectrum of an atom in an IR+XUV two-color laser field," Phys. Rev. A **88**(4), 043435 (2013).
44. K. Zhang, M. Liu, B.-B. Wang, Y.-C. Guo, Z.-C. Yan, J. Chen, and X.-J. Liu, "Role of XUV Photons in Atomic High-Order Above-Threshold Ionization Processes in IR+XUV Two-Color Laser Fields," Chin. Phys. Lett. **34**(11), 113201 (2017).

Optics EXPRESS

45. F. Jin, H. Yang, B. Wang, L. Wei, and H. Wu, "Angular resolved above-threshold ionization spectrum of an atom in IR+XUV orthogonally polarized two-color laser fields," Opt. Express **27**(15), 20754–20762 (2019).
46. S. Düsterer, L. Rading, P. Johnsson, A. Rouzée, A Hundertmark, M. J. J. Vrakking, P. Radcliffe, M. Meyer, A. K. Kazansky, and N. M. Kabachnik, "Interference in the angular distribution of photoelectrons in superimposed XUV and optical laser fields," J. Phys. B: At., Mol. Opt. Phys. **46**(16), 164026 (2013).
47. S. Düsterer, G. Hartmann, F. Babies, A. Beckmann, G. Brenner, J. Buck, J. Costello, L. Dammann, A. De Fanis, P. Geßler, L. Glaser, M. Ilchen, P. Johnsson, A. K. Kazansky, T. J. Kelly, T. Mazza, M. Meyer, V. L. Nosik, I. P. Sazhina, F. Scholz, J. Seltmann, H. Sotoudi, J. Viefhaus, and N. M. Kabachnik, "Angle resolved photoelectron spectroscopy of two-color XUV-NIR ionization with polarization control," J. Phys. B: At., Mol. Opt. Phys. **49**(16), 165003 (2016).
48. D.-S. Guo and T. Åberg, "Quantum electrodynamical approach to multiphoton ionisation in the high-intensity H field," J. Phys. A: Math. Gen. **21**(24), 4577–4591 (1988).
49. D.-S. Guo and G. W. F. Drake, "Stationary solutions for an electron in an intense laser field II. Multimode case," J. Phys. A: Math. Gen.: Math. Gen. **25**(20), 5377–5394 (1992).
50. F. Jin, F. Li, Y. Yang, J. Chen, X. Liu, and B. Wang, "Angle-resolved photoelectron energy spectrum from the high-order above-threshold ionization process in IR+XUV two-color laser fields," J. Phys. B: At., Mol. Opt. Phys. **51**(24), 245601 (2018).
51. Ph. A. Korneev, S.V. Popruzhenko, S. P. Goreslavski, T.-M. Yan, D. Bauer, W. Becker, M. Köbel, M. F. Kling, C. Rödel, M. Wönsche, and G. G. Paulus, "Interference Carpets in Above-Threshold Ionization: From the Coulomb-Free to the Coulomb-Dominated Regime," Phys. Rev. Lett. **108**(22), 223601 (2012).
52. R. Reichle, I. Yu. Kiyan, and H. Helm, "Two-slit interference in strong-field photodetachment of H^-," J. Mod. Opt. **50**(3-4), 461–470 (2003).
53. R. Reichle, H. Helm, and I. Yu. Kiyan, "Photodetachment of H^- in a Strong Infrared Laser Field," Phys. Rev. Lett. **87**(24), 243001 (2001).